Journal of Materials Chemistry C

The role of orientation in the MEL response of OLEDs

Journal:	*Journal of Materials Chemistry C*
Manuscript ID	TC-ART-01-2021-000314.R1
Article Type:	Paper
Date Submitted by the Author:	25-Jun-2021
Complete List of Authors:	Engmann, Sebastian; NIST, ; Theiss Research, Bittle, Emily; National Institute of Standards and Technology, Richter, Lee; National Institute of Standards and Technology, Materials Mesaurment Laboratory Hallani, Rawad; King Abdullah University of Science and Technology, Solar and photovoltaics engineering research center Anthony, John; University of Kentucky, Chemistry and Advanced Carbon Materials Gundlach, David; National Institute of Standards and Technology,

The role of orientation in the MEL response of OLEDs

Sebastian Engmann[1,2], Emily G. Bittle[2], Lee J. Richter[3], Rawad K. Hallani[4,5], John E. Anthony[4], David J. Gundlach[2]

[1]*Theiss Research, La Jolla, California 92037, United States*

[2]Nanoscale Device Characterization Division, National Institute of Standards and Technology, 101 Bureau Drive, Gaithersburg, Maryland, 20899, United States

[3]Materials Science and Engineering Division, National Institute of Standards and Technology, 101 Bureau Drive, Gaithersburg, Maryland, 20899, United States

[4]Department of Chemistry, University of Kentucky, Lexington, Kentucky, 40506, United States

[5]Current address: KAUST Solar Center, King Abdullah University of Science and Technology, Thuwal 23955-6900, Kingdom of Saudi Arabia

Correspondence and requests for materials should be addressed to D.J.G. (email: david.gundlach@nist.gov) or S.E (email: s.engmann@theissresearch.org)

Keywords

Triplet Fusion, Singlet Fission, Organic Light Emitting Diodes, Small Molecule, Anthradithiophene, Rubrene, Magneto Electroluminescence

Abstract

Magneto electroluminescence (MEL) is emerging as a powerful tool to study spin dynamics in organic light emitting diodes (OLEDs). The shape of the MEL response is typically used to draw qualitative inference on the dominant process (singlet fission or triplet fusion) in the device. In this study, we develop a quantitative model for MEL and apply it to devices based on Rubrene, and three solution processable anthradithiophene emitters. The four emitters allow us to systematically vary the film structure between highly textured, poly-crystalline to amorphous. We find significant diversity in the MEL, with the textured films giving highly structured responses. We find that the additional structure does not coincide with energy anti-crossings, but intersections in the singlet character between adjacent states. In all cases the MEL can be adequately described by an extended Merrifield model. Via the inclusion of charge injection, we are able to draw additional information on underlying physics in OLED devices.

Introduction

Recently the scientific community has developed significant interest in room temperature observable spin-transport phenomena in organic materials and coherent spin processes like singlet fission (SF) and triplet fusion (TF).[1, 2] Unlike most inorganic counterparts, organic materials exhibit strong exciton binding energies and comparably long spin relaxation times[1, 3-5] that make them of interest to areas of quantum information science (QIS) as they may enable future quantum applications such as computing, transduction, or sensing. In the near term, SF could lead to an increase in performance of organic photovoltaics[6] and TF in the emission efficiency of organic light emitting diode (OLED) devices.[7] In the development of a fundamental understanding of spin-enhanced device operation[8-12], it is critical to apply quantitative models and characterization techniques to gain deeper insights into the effect of molecular structure and arrangement to spin coherence times, spin-spin interaction and spin related phenomena. Once structure property relationships are established, that knowledge can be used to selectively pursue chemical motifs that yield further improvements in relaxation and coherence.

In this report, we systematically alter the structure of the OLED emission layer to correlate the molecular arrangement to the formation of a coherent triplet-pair state. The influence of the structure will be investigated indirectly via the effect on the material's SF and TF rate, which proceed via the coherent pair state. While the structure-property relationship between charge transport and molecular packing in organic materials is well investigated,[13-19] investigations on the effect of molecular arrangement on spin-phenomena in electronic devices beyond studies on 2D materials [20, 21] is not. However, studies of SF in small molecule solutions and films have shown that the problem is inherently a dimer problem, in which a fundamental requirement is the close proximity of 2 molecules to enable interaction between spins and the formation of a coherent pair state. Noteworthy are the studies by Walker et al.[22] and Stern et al.[23] who have identified the coherent triplet pair state as an

intermediate step in SF and TF from singlet exciton to triplet excitons in solutions. Via time resolved spectroscopy techniques they were able to determine the SF and TF rate constants, quantum yields, and concentration onset at which these processes occur. The concentration in solution is equivalent to the average distance between molecules and thus excitons. It was found that SF was limited to an average molecule distance of about 7 nm to 8 nm.[22] In thin films SF and TF rates can be expected to be affected by the specific molecular arrangements and packing motifs which lead to variations in exciton-to-exciton distances and the relative orientation of spins to each other.

The goal of this work is to provide the methodology necessary for convergence between i) purely photo-physical studies governed by well-defined initial conditions and interpreted through a robust theoretical framework, and ii) thin film devices relying on charge injection with more complex, poorly defined steady state conditions and interpreted through a largely phenomenological framework.

Results

To investigate the effect on SF and TF in OLED devices with different packing motifs, we compared OLED devices made of the singlet emitters Rubrene, 2,8-difluoro-5,12-bis(4-*tert*-butyl phenylethynyl)anthra[2,3-b;6,7-b']dithiophene (DiF-tBPhE-ADT), 2,8−difluoro-5,12-bis(2-ethylhexylthienyl)anthra[2,3-b;6,7-b']dithiophene (DiF-EHT-ADT), and 2,8-Difluoro-5,12-bis(triethylsilylethynyl)anthra[2,3-b;6,7-b']dithiophene (DiF-TES-ADT). Both Rubrene and DiF-TES-ADT are well studied materials and known to be highly amorphous and poly-crystalline, respectively, when deposited via thermal evaporation. All measurements in this study were performed at room temperature and focus on the differences between the 4 materials and how they manifest the MEL response. Room temperature measurements are of particular interest for a real-world application space and distinguishes organic materials

somewhat from their inorganic counterparts requiring operation at mK to few K temperature range to observe and harness such effects.

In the following section we present device measurements obtained for the 4 emitter materials. The device structure for the OLED stack as well as the chemical structure of the emitters are shown in **Figure 1**.

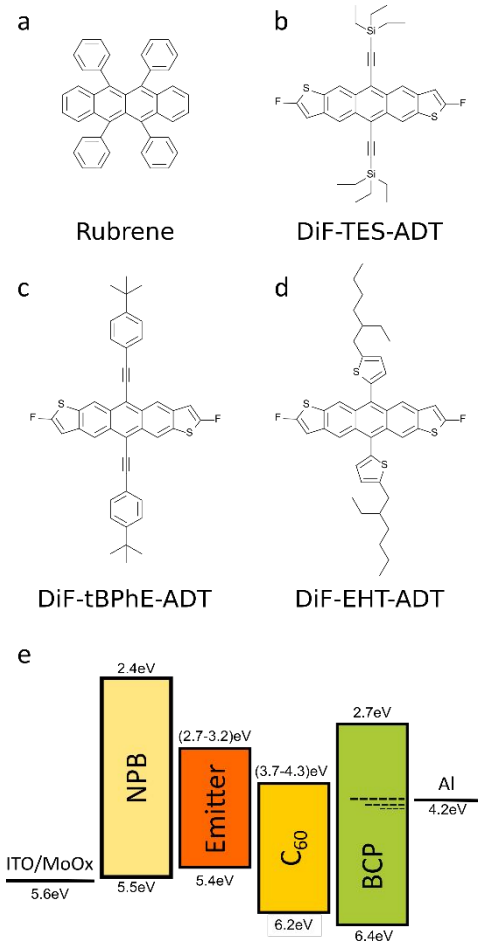

Figure 1 - Molecular Structures and Energy Level Diagrams for the investigated OLED structures
(a-d) Molecular structures of the emitter molecules under study. (e) Energy level diagrams of heterojunction devices with C_{60} acceptor layer. Highest occupied molecular orbital (HOMO) and lowest unoccupied molecular orbital (LUMO) values for values for N,N′-Bis(naphthalen-1-yl)-N,N′-bis(phenyl)benzidine (NPB) taken from Ref.[24], C_{60} taken from [10, 25-27], Bathocuproine (BCP) values taken from.[28, 29]

Besides their similar HOMO levels, all materials are expected to exhibit triplet energies that are comparable to the charge transfer (CT)-state energy for excitons formed at the donor:acceptor interface. However, only Rubrene and DiF-TES-ADT have been characterized photo-physically to a degree that triplet and coherent pair state (TT) energies are known to the

scientific community. The energetics for these two materials is summarized in **Error! Reference source not found.**. These energetic differences have implications on the balance of SF to TF as well as singlet re-formation, as discussed in detail by Yong et al.[30]

A set of current density-voltage-luminescence-characteristics (*J*-*V*-L-characteristics), of heterojunctions consisting of emitter/C_{60}, are shown in **Error! Reference source not found.**a. In agreement with earlier reports, a reduction of the turn-on voltage from about 2 V to slightly above 1 V can be observed for the Rubrene based heterojunctions compared to the homojunction without C_{60}.[10, 11, 25-27] This reduction is often attributed to TF or other higher order processes like Auger-recombination.[10, 25-27, 31] It is commonly agreed upon that TF contributes to the electroluminescence in Rubrene based devices, but the degree of TF that is observable is dependent on the dominant recombination pathways and relative recombination rates within the device and influenced by the device architecture and fabrication methods. It is only through detailed modeling[11] that the quantitative role of TF can be understood. Therefore, the band-alignment within the heterojunction device as well as potential barriers formed by the Fermi level alignment within the device is of utmost importance. The turn-on voltage is found to be strongly correlated to the device built-in potential.[11] It is to note that in the inverse case, where the device is operated as solar cell, the open circuit voltage would stronlgy limited by the built-in potential.[32] The electro-luminescence spectra are plotted in **Error! Reference source not found.**b. The spectra correspond to the respective emitter spectra and do not show a significant contribution from CT states formed at the heterojunction interface. CT-state emission is expected to be at approximately 850-900 nm in case of Dif-EHT-ADT, Rubrene[33] and DiF-TES-ADT. It is noteworthy that weak CT-state emission at 870 nm (≈1.4 eV) in Rubrene/C_{60} heterojunctions was observed with mixed interface layers but not heterojunctions with an abrupt interface.[11]

Shown in **Figure 2** are the current density dependent magneto-electroluminescence (MEL) characteristics of the 4 investigated emitters. Despite a common low luminescence turn-on voltage in heterojunction devices with C_{60} for all 4 materials, the materials substantially differ in their MEL response. The MEL response is defined as the relative change of the electro-luminescence (EL) with magnetic field compared to the 0 mT case:

$$MEL(B) = \frac{EL(B) - EL(0)}{EL(0)}.$$

The response is a unique property of electrical studies, and determined by the complex contributions of ionized (polaronic) and neutral (excitonic) state population density in TF and SF processes. The MEL response of organic thin films near zero magnetic field is commonly described by the superposition of Lorentzian, MEL ~ $B^2/(B^2+B_0^2)$, or non-Lorentzian line-shapes given by MEL ~ $B^2/(|B|+B_0)^2$ with B_0 related to hyperfine or spin-exchange interactions.[34-38] The assumption of the Lorentzian line-shape is historical and has only been shown and deduced for hyperfine coupling dominated MEL.[37] However, other processes exist and the sign of the MEL is dependent on the dominant processes within the device and differs for different device metrics or device architectures. For example, positive MEL can be observed for TF of two excitons via an intermediate coherent triplet pair state, where the luminescence increases for small magnetic fields, exhibits a single inflection point, followed by steadily decreasing MEL for large fields.[9, 39-41] An Auger or SF dominated MEL shows an inverted dependence and increasing fields lead to increasing MEL.[42, 43] Interestingly, there is a lack of literature reports of highly structured MEL responses with magnetic field direction. This is likely because most investigations to date have focused on amorphous thin films.

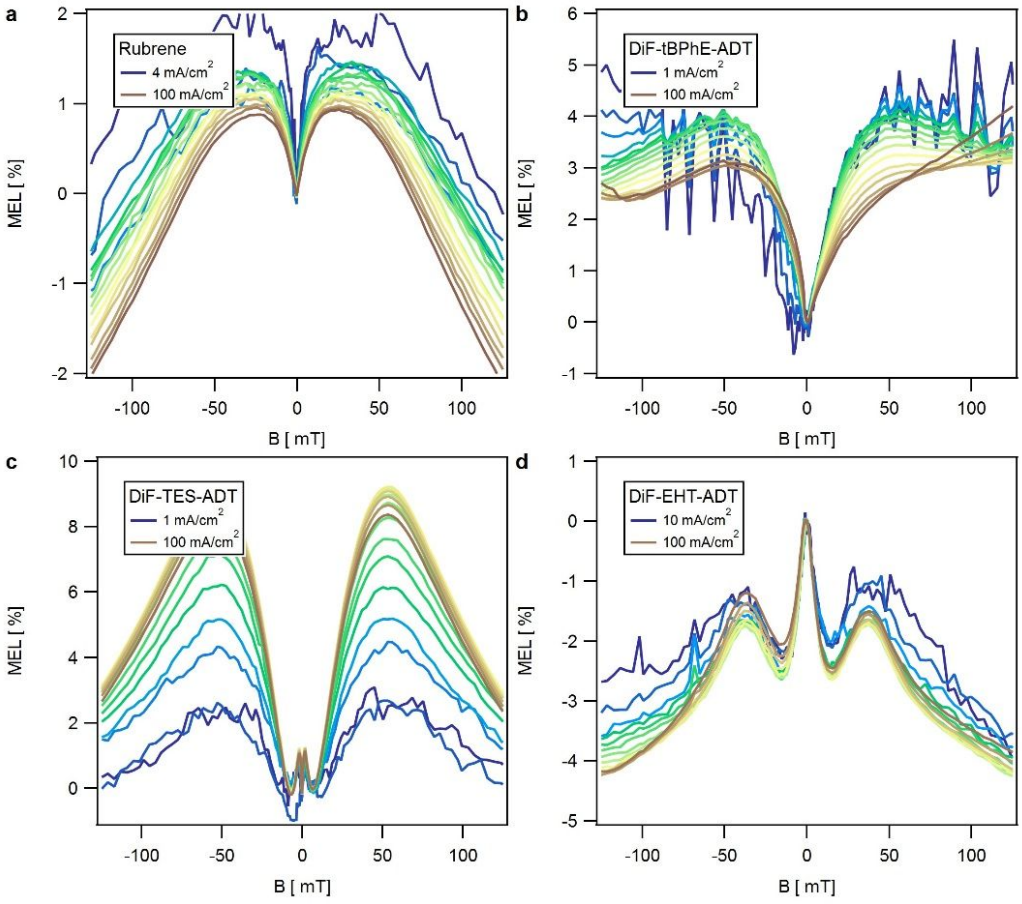

Figure 2 –MEL response of all four emitter materials
MEL response for a) Rubrene, b) DiF-tBPhE-ADT, c) DiF-TES-ADT and d) DiF-EHT-ADT based OLEDs for various injection currents between 0.1 mA/cm^2 and 100 mA/cm^2 with an exponential scaling between points. The magnetic field is parallel to the sample surface and thus perpendicular to the current through the device.

While the emitters Rubrene and DiF-tBPhE-ADT exhibit an often-reported ("conventional") MEL response shape reported for other materials exhibiting a SF or TF type of mechanism.[9, 39-41], a highly structured MEL response can be observed in the case of DiF-TES-ADT and DiF-EHT-ADT. In these cases, additional features on top the characteristic "*W*"-like or "*M*"-like shape of SF or TF dominated MEL can be observed. In all but the DiF-EHT-ADT case, the MEL response for small fields is positive, suggesting the devices are dominated by a TF type of mechanism.[9, 39-41] In all cases the position of the extrema is weakly or not magnetic field strength dependent for the different current densities. For Rubrene, the MEL maximum is located at a magnetic field of (25 to 30) mT; for DiF-tBPhE-ADT, the MEL response is wider and the maximum is observed at about (40 to 50) mT. For both cases, the

MEL decreases with increasing current density. For DiF-TES-ADT, a small local maximum is observable near 2 mT, (see **Error! Reference source not found.** for the magnified view of the low field region shown in **Figure 2**) followed by a local minimum and absolute maximum around (50 to 55) mT. The MEL response increases with increasing current density. For DiF-EHT-ADT, the MEL is negative for all investigated magnetic fields and device currents, suggesting the device is dominated by a SF type mechanism as previously mentioned. A sharp decrease is observable for small magnetic fields, followed by an increase for fields > 15 mT, a local maximum at (35 to 40) mT, and then a decrease towards large fields. The MEL response becomes more negative with increasing current density.

Detailed studies of the film morphology (see **Error! Reference source not found.** - **Error! Reference source not found.**) indicate that the MEL response (conventional for Rubrene and DiF-tBPhE-ADT; additionally structured for Dif-TES-ADT and Dif-EHT-ADT) correlates to the degree of order in the film. The conventional MEL response is seen for amorphous films, while the structured response is seen for polycrystalline films with preferential alignment; in this case, a uniaxial symmetry. We will show that the observable MEL response can be described by the spin-Hamiltonian and in particularly is determined by the zero-field parameters of the emitter molecule and the orientation relative to the external magnetic field. As such, the conclusions we will draw on these 4 emitter systems can be generalized to other materials.

Theoretical Framework

The rich phenomena reported in Figure 2 can be described by a model Hamiltonian developed below. For simplicity (and consistent with the experiments) we focus on homogeneous, and constant (or slowly varying with respect to all involved time constants - quasi constant) magnetic fields and how they translate to DC MEL measurements. We furthermore neglect temperature effects and assume that all rate constants needed are known from literature. The

detailed theoretical model is essentially the minimum model able to describe the observed differences in MEL response for the 4 material structures and ordering. Temperature effects, non-homogenious and time dependent fields are briefly adressed in the Supplementary Information – Model Extensions.

To quantitatively describe the experimental MEL, we develop a detailed model based on the triplet exciton interaction (excitonic pair) model originally introduced by Merrifield.[44] Other adaptations of Merrifield's model have proven to be viable to explaining the effects of magnetic fields on recombination processes[45], optical studies of SF and TF dynamics,[46-49] and magneto-conductance in unipolar and bipolar organic diodes[12] as well as in tetracene single crystals.[50] Weng et al. have used an polaron pair adaptation to OLEDs to obtain spin-pair dynamics and local hyperfine fields in Alq3.[51] And most recently, we were able to qualitatively describe the directional magneto-photocurrent dependence in Dif-TES-ADT single crystal transistors.[52]

In general, the approach requires the construction of the spin Hamiltonian of an interacting pair of triplets. The general form of the time-independent spin Hamiltonian for a given magnetic field and without hyperfine interaction and spin orbit coupling can be given by:

$$H = H_{magnetic} + H_{zero-field} + H_{AB} \qquad (1)$$

where $H_{magnetic} = \mu_B \sum_{i,j} g_{ij} B_i S_j$ describes the Zeeman interaction (μ_B - Bohr magnetron, g-tensor, B - external magnetic field, S - spin operator), $H_{zero-field} = \sum_{i,j} D_{i,j} S_i S_j$ the intramolecular spin-spin interaction, and $H_{AB} = \sum_{i,j} J_{ij} S_{A,i} S_{B,j}$ the intermolecular coupling of triplets on molecules A and B. The *D*-tensor can be expressed in terms of the zero field parameters *D* and *E* which correspond to an axial and to an asymmetric or transversal

component of the magnetic dipole-dipole interaction respectively. Both parameters should vary with the structure of the molecular pair (i,j). The magnetic field dependence of the coherent triplet-pair is explicitly introduced by the Zeeman term in eq. (1), which for non-zero field lifts the degeneracy within the triplet pair state manifold. The total Hamiltonian is typically represented in matrix form and solved in either the zero-field basis for triplets on a single molecule |x>, |y>, |z> or the "high field" basis |0>, |+>, |-> by diagonalization. For a 4-electron system, two solutions with spin 0 (singlets), nine solutions with spin 1 (triplets) and five solutions with spin 2 (quintets) can be found. One of the two singlet solutions is simply the product of two 2-electron singlet states, the other solution however cannot be described as a product of singlet states and instead must be described as a superposition of product pairs of 2-electron triplet states. This state is essentially a singlet correlated triplet pair ^{1}(TT) and will be of utmost interest, as out of the resulting nine possible triplet pair states ^{3}(TT), some exhibit singlet character such that a transition to (fusion) or from (fission) a singlet state is possible without the requirement for a spin-flip unlike in intersystem crossing. Thus, a transition from the singlet to the triplet pair manifold is spin-allowed and rapid TF or SF via S ↔ ^{1}(TT) ↔ ^{3}(TT) can occur. Detailed descriptions of the Hamiltonian in the zero-field basis to determine the magnetic field dependent singlet character of each state, via a projection of the eigenstate of the total Hamiltonian onto the singlet wave function, $C_{S,i} = |\langle S | \Phi_i \rangle|^2$, can be found in the literature.[44-46, 49, 52]

The determined projections are then used to scale the SF and TF rates for each of the coherent pair states. To calculate the MEL response a set of non-linear equations that describe the rates between emitter singlet and triplet states, the rates to and from CT states at the heterojunction interface and formation of excitons from injected charge carriers is solved numerically for the steady state solutions as diagrammed in **Error! Reference source not found.**. We do not distinguish between excitons (tightly coulombic bound electron-hole-pair) and polaron pairs

(weakly coulombic bound electron-hole-pair with charges likely on different molecules). Instead, we assume no transition between singlet and triplet polaron pairs and lossless transition between polaron pairs and excitons. This allows us to reduce the number of unknowns and replace the 2 formation rates from free charges to polaron pair to exciton with a single rate. Furthermore, for our model we assume that the transition from S to ^{1}(TT) is not rate limiting and can be ignored. In crystalline Hexacene this step was found to have an incoherent component which proceeds at timescales on the order of 180 fs, and a component that may couple coherently to a vibronically excited ^{1}(TT) on ultrafast timescales (<50 fs)[53]. This is orders of magnitude faster than typical SF and TF rates (see for comparison Supplementary Information: Simulation Parameter - Uniaxial Dif-TES-ADT and references therein). And lastly, we assume that no transitions within the coherent triplet pair manifold occur, e.g. no direct transitions between $^3(TT)_i \leftrightarrow {}^3(TT)_j$, despite k_BT at RT >> the energetic splitting between those states. This is equavialent to assuming a large coherence time >> SF and TF rates. As the transition within the manifold are weighted by the wavefunction overlap between the initial and final state, transitions will only be allowed between states with similar character and thermally assisted transitions within the manifold to the coherent triplet pair state with singlet character will always be more or less suppressed.

To diagonalize the Hamiltonian and calculate the singlet projections we use Matlab and EasySpin.[54] The rates of which SF and TF process occur are then proportional to a universal rate constant and the magnitude of the wave function overlap. We assume that the rates to and from the singlet exciton to the triplet manifold can be approximated by:

$$rate\{S \rightarrow {}^1(TT) \rightarrow {}^3(TT)_i\} = k_{S,TT} \cdot |\langle S \,|\, \Phi_i \rangle|^2 = k_{S,TT} \cdot C_{S,i} \qquad (2)$$

and

$$rate\{{}^3(TT)_i \rightarrow {}^1(TT) \rightarrow S\} = k_{TT,S} \cdot |\langle \Phi_i \,|\, S \rangle|^2 = k_{TT,S} \cdot C_{S,i} \qquad (3)$$

In general, the rates $k_{S,TT}$ and $k_{TT,S}$ don't have to be equal. In the following these rates will be used to derive the MEL response for various injection currents.

As we proposed earlier for Rubrene based heterojunctions, a direct path for free charge carriers (n , p) to singlet excitons (S) might exist via a bimolecular recombination process (rate constant k).[11] The extent of this pathway in the simulations can be modified by changing the fraction of charge carriers (c) that form CT states or create triplet excitons (T). Each of the generated species can undergo the usual combination and conversion processes like radiative or non-radiative recombination and transformation into another species, however we do not allow for inter system crossing (ISC) and reverse intersystem crossing (RISC). Conversion between singlet and triplet states is invoked solely via SF and TF through a coherent triplet pair state (TT).

We will neglect the recombination of the coherent triplet pair to the ground state and allow only for a decay to two triplets, one triplet and a CT-state or conversion to a singlet state. The rate equations and a schematic of the kinetic pathways are provided in **Error! Reference source not found.** and Supplementary Information: Kinetic Model - Rate equations. The set of rate equations form a system of non-linear equations and can be solved numerically. Details on the numerical solution are provided in the Supplementary Information: Details on solution of rate equations. The calculated MEL response as function of applied B-field and for a given current density (J) is then proportional to the singlet state density under these conditions:

$$MEL(B,J) = \frac{S(B,J) - S(B=0,J)}{S(B=0,J)} \quad , \qquad (4)$$

neglecting emission from triplet, charge transfer and C_{60} states. Recall that the heterojunction emission spectra shown in **Error! Reference source not found.** correspond to the singlet emission spectra. This further assumes that recombination rates within the device are not current or field dependent. The calculations for a given magnetic field orientation and a single orientation of two triplet spins are straight forward; however, the description of amorphous or semi-oriented materials requires the averaging over the distribution of the spins within a magnetic field and with respect to each other and leaves one with the choice to average the projections and calculate the observable (here MEL) with those averages or to calculate the MEL for each angle and average them in the end.[47] While more computationally expensive we chose the latter approach for the discussion of the uniaxial and isotropic case at fixed current density to guarantee the highest fidelity in the shape of the MEL response. However, for a discussion of the current density dependence we choose, without limitation, the average singlet projection approach to reduce computational time. The biggest difference between the two averaging approaches lie in the shape of the MEL response and how well the structure is preserved upon rotational averaging. As the singlet projections are current independent the experimental parameters B and J essentially create an orthogonal parameter space such that the qualitative changes in the MEL response with current density are independent of the chosen singlet projections and how they were derived, e.g. increase or decrease of MEL with current density. However, the absolute values of the MEL are dependent on the chosen averaging approach.

Before we continue, we want to point out the significant differences to existing work in the literature. Very recently Weng et al. have developed a model to derive spin-pair dynamics and local hyperfine fields from measurements of the MEL and magneto-conductance (MC) of OLEDs. Like our approach the model calculates the wavefunction overlap of singlets and triplets to derive magnetic field dependent conversion rates. However, the 2 models focus on different stages in the process from free charges to excitons and light emission. Specifically,

the prior study focuses on the effect of the magnetic field on the formation on singlet and triplet polaron pairs (precursors for the respective excitons) and their separation and reformation, this study focuses on the exciton fission and fusion. In the spin-Hamiltonian we do not include hyperfine fields into our Hamiltonian, instead we consider only the zero-field term. This approach is more in line with models derived for transient optical measurements.[46-49] It is expected that hyperfine fields contribute to the MEL at very small fields and by themselves are not able to describe the highly structured MEL response we observe (note: Weng et al focuses on magnetic fields < 0.5 mT). We will show below that the experimentally observed structure can be fully described by the zero-field-interaction. We do not want to rule out additional features or splitting of reported features due to hyperfine interaction, as both are below our measurement resolution. Further differences to existing literature lie in the developed kinetic model. While previous studies have focused on the qualitative shape of MEL or MC at a fixed current density or have drawn conclusions from the combined analysis of MEL and MC at the same fixed current density, our model extends those capabilities to the current dependent response. Unlike previous studies this allows for additional recombination and generation pathways and states, such as interface states in heterojunction devices.

Preferentially Aligned Systems

In the following we will use the poly-crystalline, uniaxial DiF-TES-ADT case to discuss features of the MEL response of an aligned system. A detailed list of all rate constants of the simulation can be found in the **Error! Reference source not found.**. It is known that DiF-TES-ADT films often are highly crystalline with the side groups facing toward the sample surface and molecules arranging in a brick-wall motif. This was confirmed by grazing incidence X-ray diffraction (GIXD) measurements shown in **Error! Reference source not**

found. and **Error! Reference source not found.**. Thus we can assume that the spins on neighboring molecules are parallel and one has to average over a distribution around the sample normal. Shown in **Figure 3** are the magnetic field dependent energy levels (eigenvalues) of the spin-Hamiltonian, the projections of the eigenvectors onto the singlet state (C_s) and the simulated MEL response for selected angles of an ordered DiF-TES-ADT OLED. The whole set of simulation parameters can be found in the supplementary information.

Highlighted in the Zeeman plots (first row of **Figure 3**) is the angle dependence of the anti-crossings (blue shaded areas) in the eigenstate energies, e.g. the "repulsion" of eigenstates with different values of the magnetic spin quantum number m_S, which are characteristic for the spin-Hamiltonian. For a zoomed in region of **Figure 3**a in the range 53 mT to 56 mT, highlighting one exemplary energy anti-crossing between adjacent states, please see **Error! Reference source not found.**.

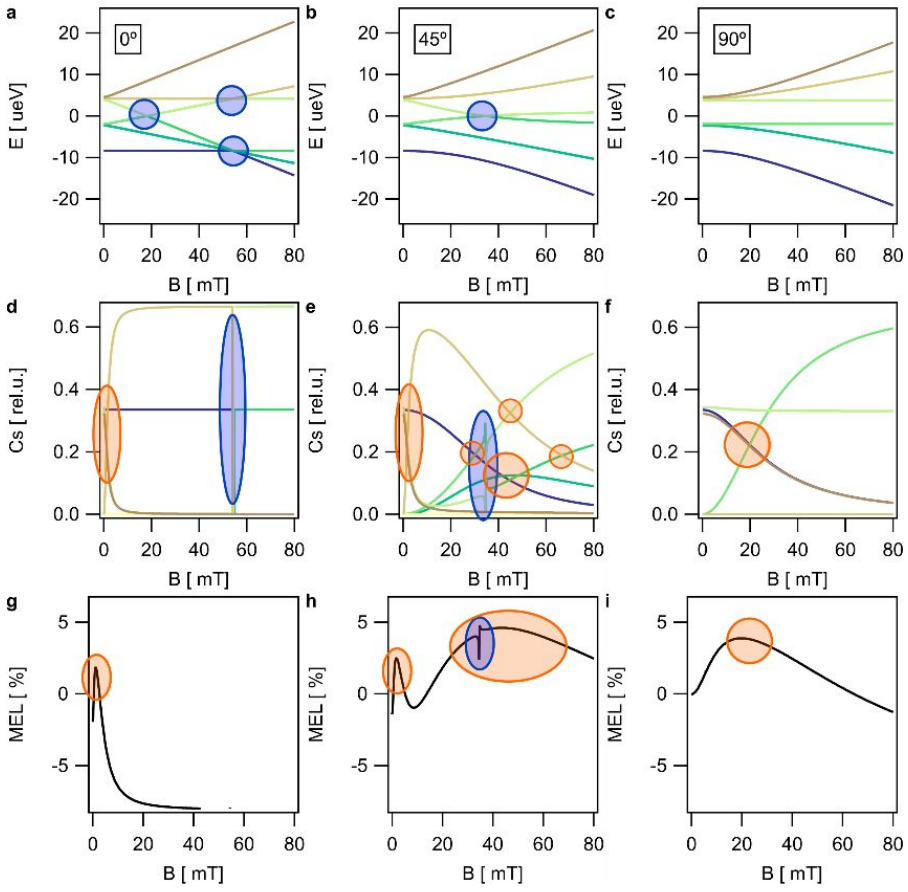

Figure 3 - Energy levels, singlet projections and MEL simulations

Energy levels, (a-c) singlet projections (d-f) and MEL (g-i) simulation for the coherent triplet-pair state in DiF-TES-ADT as function of magnetic field for selected azimuth angles. Shown are simulations for 0° (a,d,g) , 45° (b,e,h) and 90° (c,f,i) azimuth angle. States are color coded and the same coloring is used in the energy plots as well as in the singlet projections. Regions of energy anti-crossings within the energy plots are highlighted in blue shades, intersections in the singlet character between states are highlighted in orange shades. A zoomed in region (53 to 56) mT of graph a) can be found in **Error! Reference source not found.**.

The number and magnetic field position of these anti-crossings strongly depend on magnetic field direction. For example, the anti-crossing slightly below 60 mT observed for the 0° case shifts to smaller magnetic fields with increasing azimuth angle. At the anti-crossing the character of the involved states interchanges, observable as a change in slope in the Zeeman plots as well as in the projection of the state onto the singlet state (second row of **Figure 3**). In the simulated MEL a sharp resonance can be observed at these energies (see **Figure 3h** between 33 mT and 36 mT, blue shaded area), despite the fact that a real crossing does not occur. However, these resonances, that are of focus in ESR measurements, and might be of interest in the manipulation of the coherent triplet pair state densities and characters for QIS applications, are likely not observable in most experimental geometries used to measure the MEL response due to non-ideal field distributions and lack of resolution.

The experimentally observable broad features in the MEL response, on the other hand, coincide with regions of multiple intersections in the singlet projections (orange shaded areas in **Figure 3**). Near these intersections it is expected that extrema in the most populated coherent triplet pair state can be observed as the populations of the intersecting pair states rebalance through SF and TF. Unlike near the energy anti-crossings, none of the involved states changes its singlet character drastically. Often intersections between several states occur relatively close to each other in terms of magnetic field, separated only by a few mT. This can be observed in the 45° case in the 40 mT to 60 mT range where several intersections manifest into a broad MEL extremum. Again note the angle dependence of these intersections and the extrema in the simulated MEL response, see **Figure 4** for a false color plot of the MEL as function of magnetic field and field direction. By averaging over all azimuth angles,

we derive the experimentally observable MEL for a uniaxial system like our poly-crystalline DiF-TES-ADT film.

Through these simulations it is possible to extract the zero-field splitting parameters, *D* and *E*, from MEL measurements. In the DiF-TES-ADT case we found the best agreement (see Fig. 6b) for $D \approx 6.3$ μeV and $E \approx 0.2$ μeV, that are in good agreement with ODMR measurements by Yong et al. who found $D = 5.38$ μeV and $E = 0.12$ μeV.[30] While the position of the MEL features can be brought to excellent agreement, the ratio of the peaks and the overall MEL magnitude are in lesser agreement. We attribute this to not capturing the tip-tilt distribution of DiF-TES-ADT crystallites within the film and simplifications in the model that assume ideal current injection and a simplified charge carrier to singlet pathway. A simulation of the uniaxial DiF-EHT-ADT film can be found in **Error! Reference source not found.**. In the DiF-EHT-ADT case we obtained *D* and *E* values of 18 μeV and 1.2 μeV, respectively.

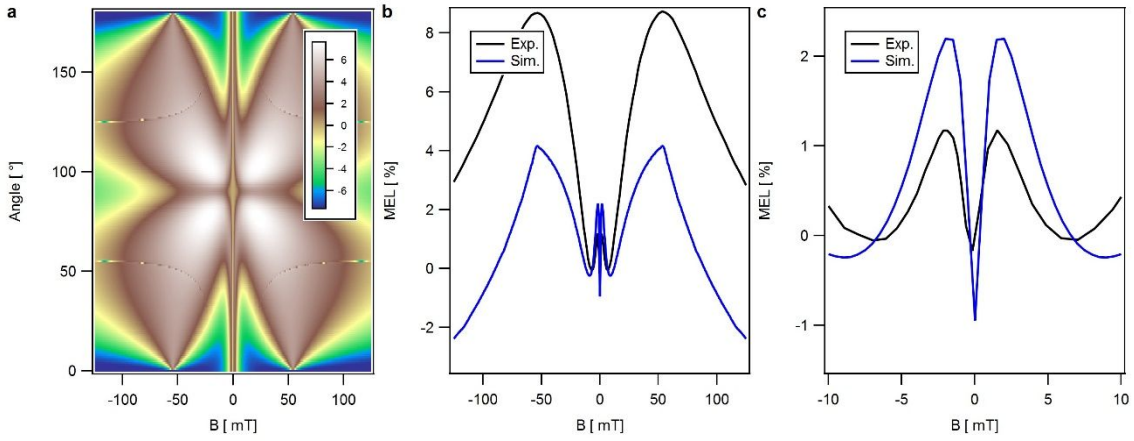

Figure 4 - MEL angle dependence and uniaxial average
False color representation of the simulated MEL response as function of azimuth angle and magnetic field (a) and comparison of the calculated uniaxial average (blue) and experimental (black) MEL response of DiF-TES-ADT at 10 mA/cm^2 current density. Shown are the whole experimental magnetic field range (b) and small B-field region (c). Note that in the simulated MEL 0% corresponds to the average of the MEL between -1 mT and 1 mT to reflect the experimental uncertainty in field homogeneity and measured field strength.

Amorphous Systems

The case of amorphous systems requires averaging the MEL response over all possible spin-orientation to each other and to the external magnetic field. This was discussed in great detail for the case of fluorescence measurements of amorphous Rubrene by Piland et al.[46] and

Tapping et al.[47] Shown in **Figure 5** is the simulated MEL response of Rubrene OLEDs. As can be seen the characteristic "*M*"-like line-shape that was experimentally observed is reasonably reproduced. The location of the observed maxima is a function of the zero-field splitting parameter *D* and *E*, where for fixed *E/D* ratio, larger values will lead to MEL extrema at larger magnetic fields.

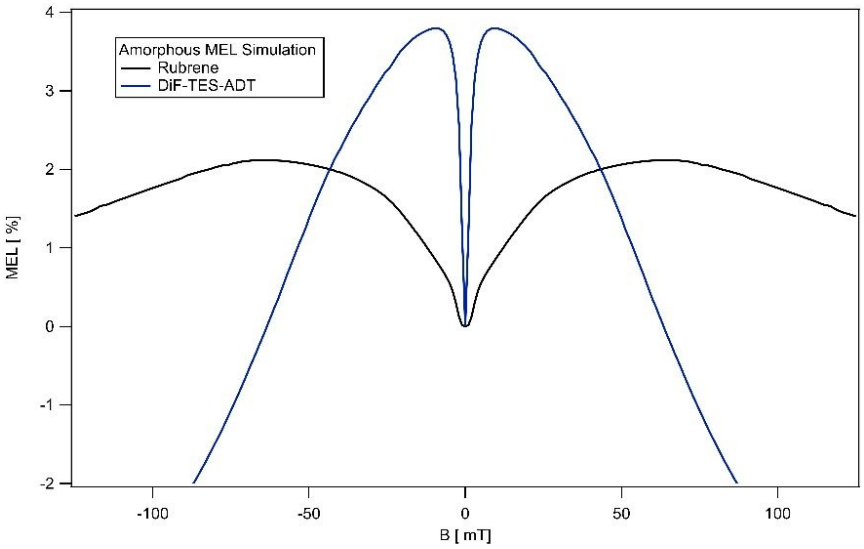

Figure 5 - MEL of Amorphous Systems
Simulated MEL response for amorphous DiF-TES-ADT (Blue) and Rubrene (black) based OLEDs.

Hypothetical systems

Also shown in **Figure 5** is the hypothetical case of "amorphous" DiF-TES-ADT using the same rates as were used in the simulations for the preferentially aligned discussion above, however averaging over all orientations. As can be seen, this leads to a loss of the additional structure that was observable in the aligned films, and instead the characteristic "*M*"-like line-shape for all amorphous materials is observed.

For completeness, we have simulated the expected MEL response for a poly-crystalline Rubrene and DiF-TES-ADT devices with ab-plane, bc-plane or ac-plane parallel to the magnetic field. The simulations can be found in the Supplementary Information - Poly-crystalline Rubrene and **Error! Reference source not found.**. Clear differences in the MEL

response with magnetic field can be observed, which originate in the molecular packing motif. Rubrene packs in a herringbone motif. Assuming that spins follow this symmetry to some extent, it becomes clear that at least one of the spins is never parallel to the magnetic field direction. In the zero-field parameter this is reflected in a comparably large E (asymmetric component of the D-tensor) *of* -2.9 μeV and E/D ratio of 0.29. On the other hand, DiF-TES-ADT packs in a brick-wall motif, with parallel molecule backbones. The high alignment of molecules parallel to a crystal plane leads to a small asymmetric component E = 0.19 μeV and E/D ratio of 0.03 and a plane in which the spins are nearly parallel to the magnetic field.

Current Density Dependence

To extend the conclusions that can be obtained by our model, we simulated the MEL response for a range of different SF and TF rates. Experimentally and theoretically one expects the rates from the singlet exciton to the coherent triplet pair state ($k_{S\text{-}TT}$), the coherent triplet pair state to triplet rate ($k_{TT\text{-}T}$), and the respective rates for the inverse processes ($k_{TT\text{-}S}$ and $k_{TT\text{-}S}$) to be strongly dependent on the energetic differences between those states. We expect the rate to be small for an endothermic process from initial to final state and significantly increased rate constant for an exothermic process. Overall, it is expected that for the exothermic energy cascade 2xT > (TT) > S TF would dominate the MEL emission, and for an endothermic (2xT < TT < S) cascade quenching of the luminescence by SF dominates the MEL response. The overall zero field SF and TF rates can be calculated from the rates between S ↔ TT ↔ T via:[49]

$$k_{SF} = \sum_i \frac{k_{S-TT} k_{TT-T} C_{S,i}}{k_{TT-T} + k_{TT-S} C_{S,i}} \qquad (5)$$

and

$$k_{TF} = \frac{1}{9}\sum_i \frac{k_{T-TT}k_{TT-T}C_{S,i}}{k_{TT-T} + k_{TT-S}C_{S,i}}, \qquad (6)$$

where it was assumed that the coherent triplet pair state cannot decay by itself or otherwise, except the conversions S ↔ TT ↔ T that correspond to SF and TF.

Table 1 summarizes the varied simulation parameters and provides the calculated SF and TF rates. A full set of simulation parameters can be found in **Error! Reference source not found.**. As can be seen from Table 1, the simulations range from TF dominated to SF dominated.

	a) dominated by TF	b) dominated by TF	c) dominated by TF	d) "balanced" SF and TF	e) dominated by SF
$k_{T\text{-}TT}$ [$cm^{-3}\ s^{-1}$]	$5\cdot10^{-15}$	$50\cdot10^{-15}$	$50\cdot10^{-15}$	$5\cdot10^{-15}$	$5\cdot10^{-15}$
$k_{S\text{-}TT}$ [s^{-1}]	$0.1\cdot10^{12}$	$0.1\cdot10^{12}$	$1\cdot10^{12}$	$1\cdot10^{12}$	$10\cdot10^{12}$
k_{SF} [s^{-1}]	$3\cdot10^{10}$	$3\cdot10^{10}$	$3\cdot10^{11}$	$3\cdot10^{11}$	$3\cdot10^{12}$
k_{TF} [$cm^{-3}\ s^{-1}$]	$1.7\cdot10^{-15}$	$1.7\cdot10^{-14}$	$1.7\cdot10^{-14}$	$1.7\cdot10^{-15}$	$1.7\cdot10^{-15}$
k_{TF} / k_{SF} [cm^{-3}]	$1.8\cdot10^{25}$	$1.8\cdot10^{24}$	$1.8\cdot10^{25}$	$1.8\cdot10^{26}$	$1.8\cdot10^{27}$

Table 1 - Varied simulation parameter the current dependent MEL response
Part of the simulation parameter used in the simulations to generate Figure 6. The constant parameters can be found in **Error! Reference source not found.**. The SF and TF rates were calculated using eq. (5) and (6). a) - e) appear in the same order as in Figure 6. Categories were chosen based on the dominant process at medium current densities.

Shown in **Figure 6** are the results of a simulation in which the singlet projections C_s used to describe the magnetic field dependence correspond to the averaged singlet projections of the uniaxial DiF-TES-ADT case reported above. However, as these projections are current independent, this choice does not lead to a loss of generality. In order to classify the simulations into broader categories, the dominant process at medium current densities was chosen. The MEL response for TF dominated devices are shown in **Figure 6a) - Figure 6**c). At very low current densities (<1 mA/cm^2 in the simulation) device emission is dominated by emission from singlets that were formed from free charge carriers. The triplet state density is

low and SF out-competes TF. However, with increasing current the injected triplet density increases and leads to a higher probability for triplets to interact and form coherent triplet pairs. This is reflected in an over-proportional increase of the coherent pair state. As more singlets are formed via TF the MEL response increases. A maximum in the coherent state density is observed at low to medium-current densities when population via SF and TF is the highest. Shortly thereafter a maximum in the singlet state density is observed, followed by a decrease in MEL. For high current densities SF effects can be neglected, and in agreement with the model by Qiao et al.[31] that described the luminescence-current dependence of Rubrene OLEDs outside a magnetic field, the triplet state density approaches $T \sim J^{1/2}$. This in turn leads to a linear dependence for the triplet pair state density and a linear luminescence dependence on field. The magnitude of the MEL is observed for the region in which the triplet state density shows the inflection point in the gradual change from $T \sim J$ *to* $T \sim J^{1/2}$. This region coincides with the region in which the singlet state density shows the largest exponent n as function of current density, $S \sim J^n$. Note that $S(J) = 1$ for $J \rightarrow 0$ (negligible TF) and $J \rightarrow \infty$ (high triplet state limit described above). Shown in **Error! Reference source not found.** are the population densities and exponents discussed above for the case shown in d) but over a wider current density window. It is notable that the current density for which the MEL maximum is observed, increases with reduced TF rate.

Increasing the rate at which singlets form the coherent triplet pair state $k_{S\text{-}TT}$, and or decreasing the rate at which the coherent triplet pair state is formed from the triplet state $k_{TT\text{-}T}$, increases the SF rate relative to the TF rate and recombination rates. With the relative increase of the relative SF rate the current density at which TF starts to outcompete SF increases. This transition region can be shifted from low **Figure 6b)** to very high current densities **Figure 6e).** At the same time the MEL becomes more negative for small device currents. The ratio of the SF to TF rate k_{TF} / k_{SF} monotonously increases for this subset. However, note that between

Figure 6a) and **Figure 6c)** the ratio of SF to TF rate is identical, however the SF rate increased relative to the recombination pathways of triplets and singlets. This illustrates the need for a detailed device model to understand the experimental MEL response.

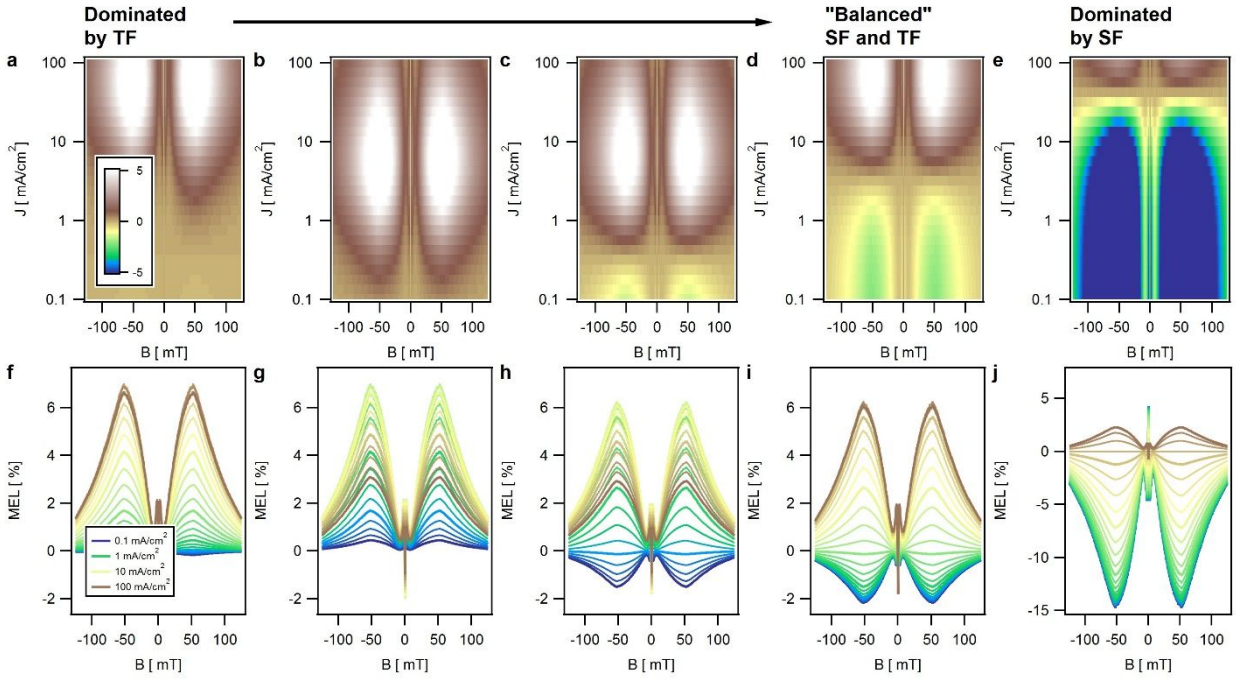

Figure 6 - Current dependent MEL for various SF and TF rates
Current dependent MEL response for current densities in the experimental relevant range of 0.1 mA/cm^2 to 100 mA/cm^2. Shown through a) to e) are false color representations and f) to j) extracted line profiles for a serious of MEL simulations with increasing SF and decreasing TF rate. The spacing between the current densities is exponential. The varied parameter are provided in Table 1. The simulations were categorized based on the dominant process at medium current densities.

Compared to the experimental observations we see a validation of a predicted maximum in MEL response at medium current densities in all devices with positive MEL response. From the relative position of the observed experimental maxima and simulation relative to each other, we suggest that the SF rate increases or TF rate decreases in the sequence Rubrene (max, MEL < 10mA/cm^2), DiF-tBPhE-ADT (max MEL ~ 10 mA/cm^2) to DiF-EHT-ADT (max. MEL ~ 30 mA/cm^2). This information cannot be drawn from line-shape analysis as commonly done for fixed injection currents that focus on positive vs. negative MEL response to distinguish between TF and SF dominated devices. Thus, the simulations extend existing capabilities and rule of thumb estimates to more quantitative and predictive probes beyond the phenomenological interpretation of J-V-L response.

Furthermore, the introduced model allows access to state densities as function of magnetic field and injection current. While optical studies of SF and TF studies on films dominate the community as they allow for well-defined generations and known singlet densities, device studies often were hindered by a lack thereof. The introduced model closes that gap and allow for a richer space of spin dependent recombination processes in electrical devices to be probed over a broader range of population densities; transitioning from trap assisted to bimolecular to higher order processes – some allowing transitioning from dark to bright excitonic states (and vice-a-versa) absent a spin flip. In principle optically and non-optically accessible phenomena and their rate constants could now be derived from parameterized model fits to the experimental MEL response. Because of the complexity of the optimization, due to the large number of variables and highly non-linear parameter dependence, this is deferred to future studies.

Unlike the devices that exhibited positive MEL response, the negative MEL response is best described by a SF quenching dominated device. However, we note that the predicted increase in MEL response and sign inversion at large current densities of Figure 6 e is not reflected in the data for DiF-EHT-ADT. Rather than the model predicted increase in MEL response with current density the experimental MEL becomes more negative. A monotonically decreasing magnitude of MEL with increasing current, in the inverted regime (Fig. 6f) is a highly unusual observation. A similar peculiar MEL response, decreasing MEL with increasing current density, was observed by Zhao et al. for exciplex based heterojunction OLEDs with an insulating interlayer compared to OLEDs without the interlayer.[55] In their report the abnormal current dependence was attributed to a confinement of the triplet state and reverse intersystem crossing RISC dominated conversion between states. This kinetic path (T)'->S is not in our present model and is inconsistent with the expected significant barrier to RISC. This suggests that an alternate kinetic origin to the anomalously negative MEL be sought.

Conclusion

This study highlights the dependence of coherent spin dependent processes on intermolecular conformation, crystal structure, and thin film orientation and how that is manifest in the structured magneto-electroluminescent response of heterostructure devices. The magnetic field strength and orientation dependence on the electroluminescence of amorphous and ordered OLED emitters is accurately reproduced by using a model based on the Merrifield approach to describe the transition rates between singlet exciton to coherent triplet pair to triplet.

The highly structured MEL response in the case of the oriented materials DiF-TES-ADT and DiF-EHT-ADT is shown to be the direct result of intersections in the magnetic field direction dependent singlet projections of the coherent triplet pair states. These intersections are a result of the contribution of the zero-field-interaction to the spin-Hamiltonian. We were able to extract the zero-field parameter D and E of DiF-TES-ADT of 6.3 μeV and 0.2 μeV, respectively. In the case of amorphous systems, the isotropic average leads to a reduction in the number of observable MEL features to the well reported "*M*"- or "*W*"-line shape. The D and E values cannot be uniquely determined in this case.

This work provides further validation for the case of charge injection and recombination in solid state devices to a point that the current dependence of the MEL response can be used to extract deeper insight into the relative dominance of SF and TF rates via a comparison to the model. The model thus provides direct insight into the triplet pair state density and lays the foundation for future in-depth studies investigating the coherent triplet pair states in poly-crystalline films in more detail. Current density and magnetic field direction dependent device measurements can be used for material screening and the determination of material constants in device relevant films. Furthermore, we show that the structure of organic materials, which can be tuned over a wide range, leads to unique magnetic field dependent properties.

Moving forward, this study provides a framework for optimizing molecular design and conformation, crystal structure, and device architecture to amplify desired spin dependent, magnetic field dependent processes. The large anisotropy in magnetic field effects observable in organic materials provides a rich space for future investigations and novel device applications exploiting the unique properties of organics. One early application of the directional MEL dependence might be magnetic field sensors for mapping applications to complement conventional probes by allowing flexible form factors, e.g. sensor patches on flexible substrates. Long-term, the strong anisotropy of magnetic field effects in organic systems could be used to selectively manipulate individual coherent states by choosing magnetic field directions and strengths that amplify characteristic features in the eigenstates and eigenvalues of the spin-Hamiltonian.

Methods

Device Fabrication

The hole injection material N,N′-Bis(naphthalen-1-yl)-N,N′-bis(phenyl)benzidine**,** (NPB), hole blocking material Bathocuproine (BCP) and emitter material Rubrene were purchased from Sigma Aldrich[1] and used as received. 2,8-difluoro-5,12-bis(4-*tert*-butyl phenylethynyl)anthra[2,3-b;6,7-b']dithiophene (DiF-tBPhE-ADT), 2,8−difluoro-5,12-bis(2-ethylhexylthienyl)anthra[2,3-b;6,7-b']dithiophene (DiF-EHT-ADT) and 2,8-Difluoro-5,12-bis(triethylsilylethynyl)-anthra[2,3-b;6,7-b']dithiophene (DiF-TES-ADT) were synthesized by the Anthony group at University of Kentucky.[56] The layered architecture of the herein investigated heterojunction devices was: Indium-tin-oxide (ITO, 145 nm)/MoOx (5 nm)/NPD (20 nm)/emitter (40 nm)/C_{60} (20 nm)/BCP(5 nm)/Al(80 nm). Devices were deposited on commercially available patterned indium tin oxide (Thin Film Devices, R_s = 15 ohms/sq). Substrates were cleaned via sonication in chloroform and isopropanol, followed by 15 min of ultraviolet/ozone treatment. Next, MoOx, NPD (Lumtec >99 %), Emitter, BCP (Lumtec >99 %), C_{60} (M.E.R. Corporation, >99.9%), and Al (R.D. Mathis, >99.99 %) were thermally evaporated using a Lesker deposition system at a base pressure of < 10^{-4} Pa connected to an N_2 purged glovebox (<1 ppm H_2O, O_2). The active area, as defined by the overlap of ITO and metal contacts, was 4 mm^2.

Device Characterization

Current density-Voltage-Luminescence, J-V-L, characteristics were measured using a Keithley 2636A source meter and Si-photodetector (Thorlabs SM1PD1B) placed on top the OLED devices. The dark current of the Si-photodetector was < 5 pA and relative

[1] Certain commercial equipment, instruments, or materials are identified in this paper in order to specify the experimental procedure adequately. Such identification is not intended to imply recommendation or endorsement by the National Institute of Standards and Technology, nor is it intended to imply that the materials or equipment identified are necessarily the best available for the purpose.

luminescence curves have been corrected for a constant background obtained in the negative bias range. Measured photodiode currents were converted to luminance values via weighting of the OLED emission spectrum by the measured detector response and luminous function. Magneto-electroluminescence, MEL, was measured with the sample placed between the poles of an electromagnet, with the magnetic field vector perpendicular to the surface normal (in the plane of the substrate). The magnetic field was measured using a Hall probe. The maximum field strength was 150 mT. EL-spectra were measured with an Ocean Optics QE65PRO spectrometer. All measurements were performed inside a N_2 purged glovebox (<1 ppm H_2O, O_2).

Author contributions

S.E. performed device optimization, device measurement, analysis and modeling. E.G.B. provided experimental support. S.E wrote the manuscript. L.J.R. and D.J.G. oversaw experimental design, analysis, and writing. J.E.A. and R.K.H. designed and synthesized ADT materials. All authors have given approval to the final version of the manuscript.

Conflicts of interest

There are no conflicts to declare.

Acknowledgements

S.E. acknowledges support from the U.S. Department of Commerce, National Institute of Standards and Technology under the financial assistance award 70NANB17H305. J.E.A. and R.K.H. acknowledge support from the National Science Foundation, award DMREF-1627428. X-ray scattering measurements were carried out at the CMS beamline of the National Synchrotron Light Source II (NSLS II), a U.S. Department of Energy (DOE) office of the Science User Facility operated for the DOE Office of Science by Brookhaven National Laboratory. We thank Dr. Ruipeng Li and Dr. Masafumi Fukuto for their assistance with X-ray scattering measurements at NSLS II.

References

1. Geng, R., et al., *A review on organic spintronic materials and devices: I. Magnetic field effect on organic light emitting diodes.* Journal of Science: Advanced Materials and Devices, 2016. **1**(2): p. 128-140.
2. Sugawara, T. and M.M. Matsushita, *Spintronics in organic π-electronic systems.* Journal of Materials Chemistry, 2009. **19**(12): p. 1738-1753.
3. Tsurumi, J., et al., *Coexistence of ultra-long spin relaxation time and coherent charge transport in organic single-crystal semiconductors.* Nature Physics, 2017. **13**(10): p. 994-998.
4. Yu, Z.G., *Spin-Orbit Coupling, Spin Relaxation, and Spin Diffusion in Organic Solids.* Physical Review Letters, 2011. **106**(10): p. 106602.
5. Nuccio, L., et al., *Importance of Spin-Orbit Interaction for the Electron Spin Relaxation in Organic Semiconductors.* Physical Review Letters, 2013. **110**(21): p. 216602.
6. Singh-Rachford, T.N. and F.N. Castellano, *Photon upconversion based on sensitized triplet–triplet annihilation.* Coordination Chemistry Reviews, 2010. **254**(21): p. 2560-2573.
7. Kondakov, D.Y., *Triplet–triplet annihilation in highly efficient fluorescent organic light-emitting diodes: current state and future outlook.* Philosophical Transactions of the Royal Society A: Mathematical, Physical and Engineering Sciences, 2015. **373**(2044): p. 20140321.
8. Xiang, C., et al., *Origin of Sub-Bandgap Electroluminescence in Organic Light-Emitting Diodes.* Small, 2015. **11**(40): p. 5439-5443.
9. Chen, Q., et al., *Determining the Origin of Half-bandgap-voltage Electroluminescence in Bifunctional Rubrene/C60 Devices.* 2016. **6**: p. 25331.
10. Pandey, A.K., *Highly efficient spin-conversion effect leading to energy up-converted electroluminescence in singlet fission photovoltaics.* 2015. **5**: p. 7787.
11. Engmann, S., et al., *Higher order effects in organic LEDs with sub-bandgap turn-on.* Nature Communications, 2019. **10**(1): p. 227.
12. Engmann, S., et al., *Reply to: Triplet-triplet annihilation in rubrene/C60 OLEDs with electroluminescence turn-on breaking the thermodynamic limit.* Nature Communications, 2019. **10**(1): p. 4684.
13. Bässler, H. and A. Köhler, *Charge Transport in Organic Semiconductors*, in *Unimolecular and Supramolecular Electronics I: Chemistry and Physics Meet at Metal-Molecule Interfaces*, R.M. Metzger, Editor. 2012, Springer Berlin Heidelberg: Berlin, Heidelberg. p. 1-65.
14. Coropceanu, V., et al., *Charge Transport in Organic Semiconductors.* Chemical Reviews, 2007. **107**(4): p. 926-952.
15. Li, Y., V. Coropceanu, and J.-L. Brédas, *Charge Transport in Crystalline Organic Semiconductors*, in *The WSPC Reference on Organic Electronics: Organic Semiconductors*. p. 193-230.
16. Liu, C., et al., *A unified understanding of charge transport in organic semiconductors: the importance of attenuated delocalization for the carriers.* Materials Horizons, 2017. **4**(4): p. 608-618.
17. Troisi, A. and G. Orlandi, *Dynamics of the Intermolecular Transfer Integral in Crystalline Organic Semiconductors.* The Journal of Physical Chemistry A, 2006. **110**(11): p. 4065-4070.
18. Vehoff, T., et al., *Charge Transport in Organic Crystals: Role of Disorder and Topological Connectivity.* Journal of the American Chemical Society, 2010. **132**(33): p. 11702-11708.

19. Bittle, E.G., et al., *Correlating anisotropic mobility and intermolecular phonons in organic semiconductors to investigate transient localization.* Communications Physics, 2019. **2**(1): p. 29.
20. Wang, S., et al., *Independent degrees of freedom in two-dimensional materials.* Physical Review B, 2020. **101**(8): p. 081414.
21. Wang, S., M.S. Ukhtary, and R. Saito, *Strain effect on circularly polarized electroluminescence in transition metal dichalcogenides.* Physical Review Research, 2020. **2**(3): p. 033340.
22. Walker, B.J., et al., *Singlet exciton fission in solution.* Nature Chemistry, 2013. **5**(12): p. 1019-1024.
23. Stern, H.L., et al., *Identification of a triplet pair intermediate in singlet exciton fission in solution.* Proceedings of the National Academy of Sciences, 2015. **112**(25): p. 7656-7661.
24. Yang, J., C.K. Suman, and C. Lee, *Effect of type-II quantum well of m-MTDATA/α-NPD on the performance of green organic light-emitting diodes.* Microelectronics Journal, 2009. **40**(1): p. 63-65.
25. He, S.J. and Z.H. Lu, *Ultralow-voltage Auger-electron-stimulated organic light-emitting diodes.* Journal of Photonics for Energy, 2016. **6**(3): p. 12.
26. Pandey, A.K. and J.-M. Nunzi, *Upconversion injection in rubrene/perylene-diimide-heterostructure electroluminescent diodes.* Applied Physics Letters, 2007. **90**(26): p. 263508.
27. Han, S., Y. Yuan, and Z.-H. Lu, *Highly efficient organic light-emitting diodes with metal/fullerene anode.* Journal of Applied Physics, 2006. **100**(7): p. 074504.
28. Yoshida, H., *Electron Transport in Bathocuproine Interlayer in Organic Semiconductor Devices.* The Journal of Physical Chemistry C, 2015. **119**(43): p. 24459-24464.
29. Lee, J., et al., *Electron transport mechanism of bathocuproine exciton blocking layer in organic photovoltaics.* Physical Chemistry Chemical Physics, 2016. **18**(7): p. 5444-5452.
30. Yong, C.K., et al., *The entangled triplet pair state in acene and heteroacene materials.* Nature Communications, 2017. **8**: p. 15953.
31. Qiao, X., et al., *Electrical pumped energy up-conversion: A non-linear electroluminescence process mediated by triplet-triplet annihilation.* Organic Electronics, 2017. **46**: p. 1-6.
32. Nolasco, J.C., et al., *Understanding the open circuit voltage in organic solar cells on the basis of a donor-acceptor abrupt (p-n++) heterojunction.* Solar Energy, 2019. **184**: p. 610-619.
33. He, S.-J., et al., *Nonradiative Charge-Transfer Exciton Recombination at Organic Heterojunctions.* The Journal of Physical Chemistry C, 2016. **120**(38): p. 21325-21329.
34. He, L., et al., *Magnetophotoluminescence line-shape narrowing through interactions between excited states in organic semiconducting materials*. Vol. 89. 2014.
35. Bobbert, P.A., et al., *Bipolaron Mechanism for Organic Magnetoresistance.* Physical Review Letters, 2007. **99**(21): p. 216801.
36. Mermer, Ö., et al., *Large magnetoresistance in nonmagnetic $\ensuremath{\pi}$-conjugated semiconductor thin film devices.* Physical Review B, 2005. **72**(20): p. 205202.
37. Sheng, Y., et al., *Hyperfine interaction and magnetoresistance in organic semiconductors.* Physical Review B, 2006. **74**(4): p. 045213.

38. Shakya, P., et al., *The magnetic field effect on the transport and efficiency of group III tris(8-hydroxyquinoline) organic light emitting diodes.* Journal of Applied Physics, 2008. **103**(10): p. 103715.
39. Johnson, R.C., et al., *Effects of Magnetic Fields on the Mutual Annihilation of Triplet Excitons in Molecular Crystals.* Physical Review Letters, 1967. **19**(6): p. 285-287.
40. Liu, R., et al., *Magnetic field dependent triplet-triplet annihilation in Alq3-based organic light emitting diodes at different temperatures.* Journal of Applied Physics, 2009. **105**(9): p. 093719.
41. Lei, Y.L., et al., *Driving current and temperature dependent magnetic-field modulated electroluminescence in Alq3-based organic light emitting diode.* Organic Electronics, 2009. **10**(5): p. 889-894.
42. Bouchriha, H., et al., *Magnetic field dependence of singlet exciton fission and fluorescence in crystalline tetracene at 300 K.* J. Phys. France, 1978. **39**(3): p. 257-271.
43. Smith, M.B. and J. Michl, *Singlet Fission.* Chemical Reviews, 2010. **110**(11): p. 6891-6936.
44. Merrifield, R.E., *Magnetic effects on triplet exciton interactions.* Pure and Applied Chemistry, 1971. **27**(3): p. 481-498.
45. Timmel, C.R., et al., *Effects of weak magnetic fields on free radical recombination reactions.* Molecular Physics, 1998. **95**(1): p. 71-89.
46. Piland, G.B., et al., *Magnetic Field Effects on Singlet Fission and Fluorescence Decay Dynamics in Amorphous Rubrene.* The Journal of Physical Chemistry C, 2013. **117**(3): p. 1224-1236.
47. Tapping, P.C. and D.M. Huang, *Comment on "Magnetic Field Effects on Singlet Fission and Fluorescence Decay Dynamics in Amorphous Rubrene".* The Journal of Physical Chemistry C, 2016. **120**(43): p. 25151-25157.
48. Piland, G.B. and C.J. Bardeen, *Reply to "Comment on 'Magnetic Field Effects on Singlet Fission and Fluorescence Decay Dynamics in Amorphous Rubrene'".* The Journal of Physical Chemistry C, 2016. **120**(43): p. 25158-25160.
49. Burdett, J.J., G.B. Piland, and C.J. Bardeen, *Magnetic field effects and the role of spin states in singlet fission.* Chemical Physics Letters, 2013. **585**: p. 1-10.
50. Jang, H.-J., et al., *Electrical Detection of Singlet Fission in Single Crystal Tetracene Transistors.* ACS Nano, 2019. **13**(1): p. 616-623.
51. Weng, Z., W.P. Gillin, and T. Kreouzis, *Fitting the magnetoresponses of the OLED using polaron pair model to obtain spin-pair dynamics and local hyperfine fields.* Scientific Reports, 2020. **10**(1): p. 16806.
52. Bittle, E.G., et al., *Measuring the impact of spin-triplet exciton orientation on photocurrent in an organic transistor.* Journal of Materials Chemistry C, 2021.
53. Monahan, N.R., et al., *Dynamics of the triplet-pair state reveals the likely coexistence of coherent and incoherent singlet fission in crystalline hexacene.* Nature Chemistry, 2017. **9**(4): p. 341-346.
54. Stoll, S. and A. Schweiger, *EasySpin, a comprehensive software package for spectral simulation and analysis in EPR.* Journal of Magnetic Resonance, 2006. **178**(1): p. 42-55.
55. Zhao, X., et al., *Direct observation of reverse intersystem crossing from fully confined triplet exciplexes using magneto-electroluminescence.* Journal of Materials Chemistry C, 2019. **7**(35): p. 10841-10850.
56. Hallani, R.K., *Designing Anthradithiophene Derivatives Suitable For Applications in Organic Electronics and Optoelectronics*, in *Chemistry*. 2015, University of Kentucky: https://uknowledge.uky.edu/chemistry_etds/61.

57. Ma, L., et al., *Singlet fission in rubrene single crystal: direct observation by femtosecond pump-probe spectroscopy.* Physical Chemistry Chemical Physics, 2012. **14**(23): p. 8307-8312.
58. Miyata, K., et al., *Coherent singlet fission activated by symmetry breaking.* Nature Chemistry, 2017. **9**: p. 983.
59. Ward, J.W., et al., *Tailored interfaces for self-patterning organic thin-film transistors.* Journal of Materials Chemistry, 2012. **22**(36): p. 19047-19053.
60. Poole, C.P., H.A. Farach, and W.K. Jackson, *Standardization of convention for zero field splitting parameters.* The Journal of Chemical Physics, 1974. **61**(6): p. 2220-2221.
61. 2021 [cited 2021; Available from: https://easyspin.org/easyspin/documentation/.
62. Ryasnyanskiy, A. and I. Biaggio, *Triplet exciton dynamics in rubrene single crystals.* Physical Review B, 2011. **84**(19): p. 193203.
63. Wurfel, P., *The chemical potential of radiation.* Journal of Physics C: Solid State Physics, 1982. **15**(18): p. 3967.
64. Nie, H., et al., *Modulation of Aggregation-Induced Emission and Electroluminescence of Silole Derivatives by a Covalent Bonding Pattern.* Chemistry – A European Journal, 2015. **21**(22): p. 8137-8147.
65. Lee, T.W., et al., *Self-Organized Gradient Hole Injection to Improve the Performance of Polymer Electroluminescent Devices.* Advanced Functional Materials, 2007. **17**(3): p. 390-396.
66. Lee, T.-W., et al., *Hole-injecting conducting-polymer compositions for highly efficient and stable organic light-emitting diodes.* Applied Physics Letters, 2005. **87**(23): p. 231106.
67. Wetzelaer, G.A.H., et al., *Origin of the dark-current ideality factor in polymer:fullerene bulk heterojunction solar cells.* Applied Physics Letters, 2011. **99**(15): p. 153506.